Improved interconnecting layer for perovskite-organic tandem solar cells

Yun Xiao[a§], Tianyu Huang[b§], Nan Chen[c§], Peng Chen[b]*, Deying Luo[d], Xin Jiang[e], Xiaohan Jia[f], Juntao Hu[g], Dengke Wang[h], Pascal Kaienburg[a], Suhas Mahesh[a,i], Anna Jungbluth[a], Rui Su[j], Congmeng Li[k], Qiang Lou[l], Chen Yang[b], Bingjun Wang[a], Irfan Habib[a], Hao Ye[a], Hang Zhou[l], Hui Li[k,m], Lei Meng[e], Xiaojun Li[e], Hongyu Yu[n], Moritz Riede[a], Zheng-Hong Lu[h,i], Rui Zhu[b,o,p]*, Henry J. Snaith[a]*

[a]Clarendon Laboratory, Department of Physics, University of Oxford, Oxford OX1 3PU, United Kingdom

[b]State Key Laboratory for Artificial Microstructure and Mesoscopic Physics, School of Physics, Frontiers Science Center for Nano-optoelectronics & Collaborative Innovation Center of Quantum Matter, Peking University, Beijing 100871, China

[c]School of Microelectronics, Southern University of Science and Technology, Shenzhen 518055, China

[d]International Institute for Interdisciplinary and Frontiers, Beihang University, Beijing 100191, China

[e]Beijing National Laboratory for Molecular Sciences, CAS Key Laboratory of Organic Solids, Institute of Chemistry, Chinese Academy of Sciences, Beijing 100190, China

[f]Cavendish Laboratory, Department of Physics, University of Cambridge, Cambridge CB3 0HE, United Kingdom

[g]Department of Physics, Mathematics and Computer Science, Faculty of Basic Medical Science, Kunming Medical University, Kunming 650500, China

[h]Department of Physics, Center for Optoelectronics Engineering Research, Yunnan University, Kunming 650091, China

[i]Department of Materials Science and Engineering, University of Toronto, Toronto M5S 3E4, Canada

[j]Department of Materials Science and Engineering, North Carolina State University, Raleigh NC 27695, USA

[k]Institute of Electrical Engineering, Chinese Academy of Sciences, Beijing 100190,

China

[l]School of Electronic and Computer Engineering, Peking University Shenzhen Graduate School, Shenzhen 518055, China

[m]Beijing National Laboratory for Condensed Matter Physics, Institute of Physics, Chinese Academy of Sciences, Beijing 100190, China

[n]School of Integrated Circuits, Shenzhen Polytechnic University, Shenzhen 518055, China

[o]Key Laboratory for Advanced Optoelectronic Integrated Chips of Jiangsu Province, Peking University Yangtze Delta Institute of Optoelectronics, Nantong, Jiangsu 226010, China

[p]Collaborative Innovation Center of Extreme Optics, Shanxi University, Taiyuan, Shanxi 030006, China

*E-mail: iamchenpeng@pku.edu.cn; iamzhurui@pku.edu.cn; henry.snaith@physics.ox.ac.uk

§Y.X., T.H., and N.C. contributed equally to this work.

Abstract

Monolithic perovskite-organic tandem solar cells (POTSCs) have attracted considerable attention in recent years due to their compatible fabrication routes and advances in single-cell efficiencies. To further boost the performance of POTSCs, reducing the voltage losses that mainly arise from wide bandgap (WBG, >1.7 eV) perovskite subcells and interconnecting layers (ICLs) is critical. Here, a new ICL with a configuration of C_{60}/YbO_x/Au/MoO_x is demonstrated for constructing the monolithic POTSC. The YbO_x-based ICL benefits an ohmic contact and high transparency, resulting in improved POSTCs performance. The champion device presents a PCE of 23.2% owing to a high V_{OC} of 2.11 V (approximately equal to the sum of individual V_{OC}s of the subcells) without compromising the short-circuit current density and fill factors. This work opens

an avenue for developing efficient ICLs in the POTSCs.

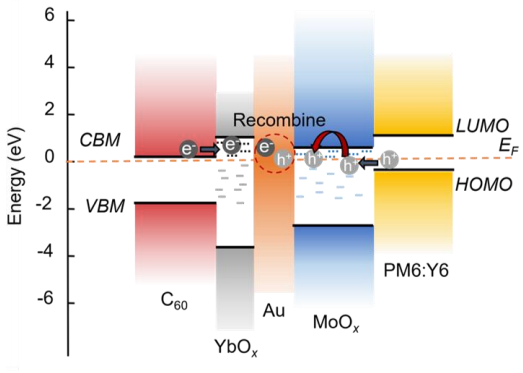

In recent years, perovskite solar cells have made impressive progress in power conversion efficiency (PCE). The champion perovskite solar cell (PSC) so far has recorded 27.0% of PCE, which is comparable to the record of single-junction silicon solar cells and approaching the theoretical detailed balanced limit of 33.7%.[1-2] To further harness the incident light and increase the PCE surpassing the limit, great efforts are dedicated to fabricating tandem solar cells (TSCs) which comprise multiple light absorbers, typically one wide bandgap (WBG) absorber and one narrow bandgap (NBG) absorber that are responsible for absorbing short-wavelength and long-wavelength photons, respectively.[3-6] Perovskite and organic solar cells (PSCs, OSCs) share similar layered device structures and solution-processable fabrication routes, making it technically encouraging to fabricate monolithic perovskite-organic tandem solar cells (POTSCs).[7] Furthermore, the solvents used for dissolving perovskite precursors, e.g., dimethylformamide (DMF), dimethyl sulfoxide (DMSO), are orthogonal to those used for organic films, e.g., chlorobenzene.[8] This feature makes the processing steps less demanding when depositing rear absorbers and provides more flexibility in interconnecting layers (ICLs) design and fabrication. Historically, the research in POTSCs dates back to 2015, which obtained a modest PCE of 10.2%.[9] Due to the domination of [6,6]-phenyl-C61-butyric acid methyl ester (PCBM) in early-stage OSCs, the development of POTSCs has long been limited by the unmatched absorption range and less efficient near-infrared absorption. In recent years, the breakthrough in non-

fullerene acceptors (NFAs) inspired the advance of OSCs since these NFA-based OSCs own NBG of 1.2~1.4 eV with strong absorption in the near-infrared region and small voltage loss.[10-12] Therefore, the lifts in both short-circuit current density (J_{SC}) and open-circuit voltage (V_{OC}) have taken the PCE a major step forward exceeding 20%.[13-15] The achievement in OSCs sees the promise in further promoting monolithic POTSCs.

As the monolithic TSCs are connected in series, it is necessary to reduce voltage loss in each component to maximize the total V_{OC}[16-17]. In a typical POTSC, the perovskite subcell based on a WBG perovskite (>1.7 eV) generally suffers from a large V_{OC} deficit, which is regarded as one challenging factor hindering the achievement of efficient POTSCs. This is mainly attributed to photo-induced halide segregation, trap-assisted non-radiative recombination in perovskite films, and poor heterojunction at the perovskite/charge transporting layers.[18-22] In contrast, the V_{OC} deficit in a mid-bandgap perovskite (~1.5 eV) can be reduced down to below 0.4 V.[23-25] Nevertheless, it is still difficult to obtain a V_{OC} above 1.30 V in a WBG perovskite, indicating a V_{OC} deficit greater than 0.4 V and thus limiting the overall device performance.

In addition to light absorbers, the ICL also plays a non-negligible role. Ideally, the ICL design should meet the criteria in all three aspects: ohmic contact, minimal parasitic absorption, and mechanically robust.[21, 26-27] Typically, the ICLs in perovskite-based TSCs are configured in sandwich stacks: the electron transporting layer (ETL)/charge recombination layer (CRL)/hole transporting layer (HTL). However, the state-of-the-art ICL usually adopts SnO_x as the ETL, which is processed by the time-consuming atomic-layer-deposition (ALD) technique.[4, 6] Therefore, the innovation in ICL design catering to both performance and technical considerations is necessary. In this work, we first suppressed the V_{OC} deficit through a surface treatment strategy for WBG perovskite, leading to the improved n-type interface, boosting the V_{OC} over 1.3 V with a reduced V_{OC} deficit of 0.47 V. The champion WBG perovskite cell delivered a PCE over 20% with a J_{SC} of 18.5 mA cm^{-2} and a fill factor (FF) of 0.83. Taking the WBG

perovskite as the front subcell, we further demonstrated a facile ICL design using an ultrathin layer of YbO_x for POTSCs. Yb can be easily thermal-evaporated and oxidized into a metal oxide film, working as the buffer layer.[28-29] The low work function of YbO_x enables it to form an ohmic contact at the ETL/CRL interface, thereby facilitating electron transport. Then the full POTSC was fabricated in the p-i-n structure as follows: ITO/NiO_x/self-assembled monolayer (SAM)/perovskite/C_{60}/YbO_x/Au/MoO_x/organic/PFN-Br/Ag. A WBG (1.77 eV) perovskite $FA_{0.83}Cs_{0.17}Pb(I_{0.6}Br_{0.4})_3$ and an NBG (1.33 eV) organic blend of PM6:Y6 were used as the front and rear absorbers, respectively. Due to the well-matched subcells and effective ICL, the champion POTSC delivered a PCE of 23.2% with an impressive V_{OC} of 2.11 V, a J_{SC} of 13.9 mA cm^{-2}, and an FF of 0.79. The high V_{OC} of POTSCs indicates that two subcells were efficiently connected by the newly designed ICL, where the voltage drop in the ICL is negligible. Also, as the whole ICL is fully thermal-evaporated, the processing route can be greatly simplified, making it strongly competitive in scalable production.

We started with preparing WBG perovskite absorbers using the composition $FA_{0.83}Cs_{0.17}Pb(I_{0.6}Br_{0.4})_3$ reported in previous work.[30] During the preparation of perovskite films, anti-solvents containing 1-butyl-3-methylimidazolium tetrafluoroborate ($BMIMBF_4$) ionic liquid additive were used to suppress halide ion migration for enhanced stability[31] while concurrently modulating crystallization kinetics toward homogeneous morphology.[32] Subsequently, the films were treated with phenethylammonium iodide (PEAI) and methylammonium iodide (MAI) in isopropanol/N,N-dimethylformamide (IPA/DMF, 99.5:0.5 v/v). PEAI may form a low-dimensional perovskite layer that passivates interfacial defects and optimizes energy-level alignment, while MAI balances the 2D/3D phase ratio to prevent charge transport losses.[33] The polar DMF additive facilitates PEAI penetration into grain boundaries,[34] synergistically establishing a graded 2D/3D heterojunction for improved photovoltaic performance. We first checked the morphology and structural information. The

scanning electron microscopy (SEM) images (Figure 1a,b, Figure S1) have clearly shown that the brighter (electron-dense) crystallites have been removed after the treatment. From the X-ray diffraction (XRD) results (Figure 1c), it is found that the peak at 12.7° corresponding to PbI_2 is no longer visible, indicating that most of the excess unreacted PbI_2 has been "digested".[35] Beyond the surface, there is no distinct change in the XRD patterns, implying no structural variation occurs in the perovskite bulk. The ultraviolet-visible (UV-vis) absorption spectra also confirm that there is no distinct change in bandgap after the treatment (Figure S2). These results suggest that the surface treatment can effectively polish the perovskite surface while making little change over the bulk structure.

To assess the effect of the surface treatment on the interfacial passivation, we performed the time-resolved photoluminescence (TRPL) decay and electroluminescence measurement (Figure 1d,e). The TRPL decay demonstrates that treated films exhibit a much longer carrier lifetime than the control ones (Table S1), indicating the effective non-radiative recombination suppression achieved by the surface treatment.[36-37] From the electroluminescence (EL) measurement where PSCs are operating as a light-emitting diode, it is clear that much higher EL intensities and external electroluminescence quantum efficiency (EQE_{EL}) were recorded for treated samples than control ones (Figure 1e, Figure S3). By passivating the surfaces, the treatment strongly reduces the interfacial non-radiative recombination losses, which thereby contribute to a higher V_{OC}.[36] The effective surface passivation leads to the enhancement in overall device performance (Table 1 and Figure S4). The current-density voltage (*J*–*V*) scan under AM1.5G illumination (100 mW cm^{-2}) shows that the champion-treated cell obtained a PCE over 20%, a V_{OC} over 1.3 V with a small voltage loss of 0.46 V, which is among all the most efficient WBG cells with a similar bandgap (Figure 1f).[19-20, 38-40] The external quantum efficiency (EQE) spectra are consistent with the trend in the *J*–*V* scans of control and treated WBG PSCs (Figure S5). These results prove the effectiveness of this treatment strategy in enhancing the performance of WBG PSCs.

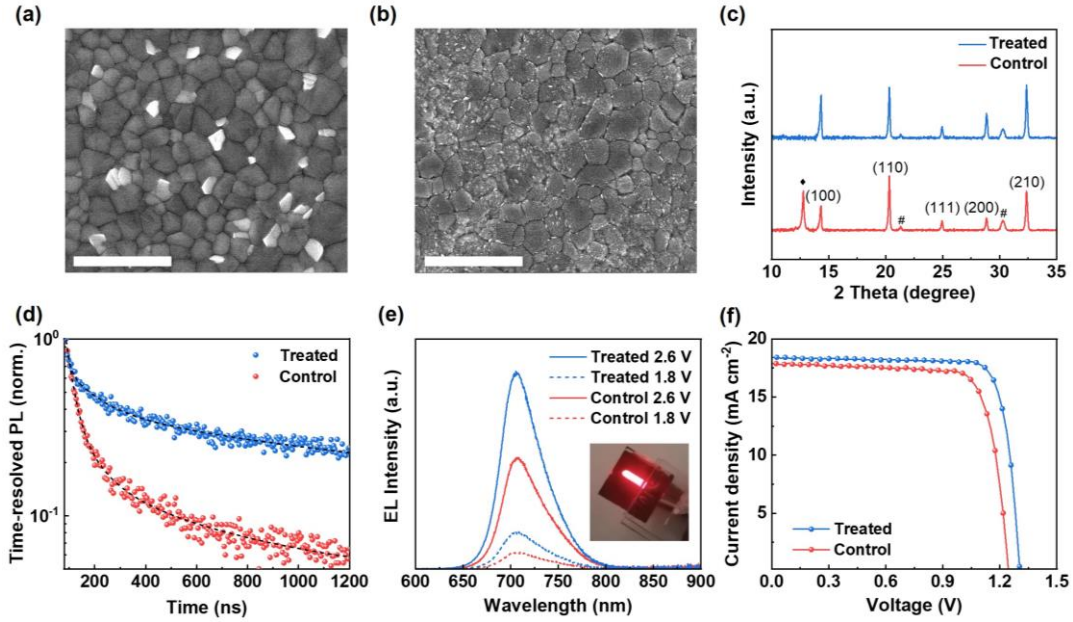

Figure 1. Surface treatment for wide bandgap (WBG) perovskite. Scanning electron microscopy (SEM) images of control (a) and treated (b) perovskite films, scale bar, 1 μm. (c) X-ray diffraction (XRD) spectra of treated and control perovskite films. Indices are for the perovskite phase, and secondary phases are marked: PbI_2 with ♦, ITO with #. (d) Time-resolved photoluminescence (TRPL) decays for treated and control perovskite films prepared on ITO substrates. (e) Electroluminescence (EL) spectra of WBG PSCs under different biases. Inset: the photograph of the WBG PSC operating as a light-emitting diode under a bias ~3 V. (f) *J*–*V* curves of the treated and control WBG PSCs.

Table 1. Device performance of champion WBG PSCs without (control) and with surface treatment (treated).

	V_{OC} (V)	J_{SC} (mA cm^{-2})	FF	PCE (%)
Control	1.25	17.9	0.78	17.3
Treated	1.30	18.5	0.83	20.1

Based on the enhanced WBG perovskite cells, we next moved on to the design of NBG cells and ICLs for the fabrication of full POTSCs. The choice of NBG absorber should

take two factors into account: strong light absorption in the near-infrared (NIR) region and small voltage loss. To pair with the 1.77 eV perovskite, an NBG organic blend of PM6:Y6 with a bandgap of 1.33 eV was chosen.[41] The organic absorber consists of a polymer PM6 as the donor and a non-fullerene small molecular Y6 as the acceptor, which has been widely proven to be efficient and reliable.[20, 26, 42] It has two absorption peaks in 550-850 nm, ensuring the complementary absorption of low-energy incident photons (Figure 2a). We fabricated NBG OSCs with a device structure of ITO/MoO_x/PM6:Y6/PFN-Br/Ag and achieved a high V_{OC} of 0.85 V (Table 2). The fabricated OSCs exhibit a wide photon-to-electron conversion range from 300 nm to 960 nm based on EQE spectra (Figure S6). It should be noted that to pair with the NBG organic back cells and achieve complementary light absorption, the thickness of perovskite front cells has been optimized (See detailed discussion below), which is different from the optimal fabrication protocol of single-junction WBG PSCs. To be specific, the concentration of perovskite precursors has been reduced from 1.4 M to 1.0 M to realize a thinner perovskite light absorber. Despite the beneficial effect of constructing TSCs, this could reduce the PCE of WBG perovskite subcells, possibly due to the reduced light absorption, varied film morphology, etc. (Table 2).

To connect the two subcells into one monolithic device, the design of ICLs should stress both the functionality (i.e., electrical and optical considerations) and practicality (i.e., challenges encountered during the processing). The electrical consideration requires materials with suitable energy levels and high conductivity so that electrons and holes can be effectively extracted and annihilated quickly. The optical consideration refers to the “relative transparency” i.e., materials should be highly transparent in the interested range in order to enable sufficient photons to pass. Last but even more important is that the processing of the latter layers shall not damage the former layers, e.g., high-energy bombardment and solvent dissolving. Furthermore, stable and cost-effective materials and facile processing methods are preferred. Based on these factors, firstly, we compared several ICLs with different CRLs (Figure 2b). The one solely employed

sputtered aluminum-doped zinc oxide (AZO) as the CRL demonstrates a severe S-shaped *J–V* curve possibly due to the misaligned energy levels and thereby non-ohmic contact within the ICL stack. Replacing the AZO with Au can mitigate the S-kink. Whereas, the utilization of the bathocuproine (BCP) buffer layer in ICL, which is high-cost and thermally unstable, would impede further application.[28] Here we developed the ICL based on a low-cost YbO_x layer by thermal evaporation. The *J–V* scans on the ICL diode samples confirmed that the deposition of YbO_x reduces the Schottky barrier and enables the ohmic connection (Figure 2c). Due to the high cost and additional fabrication procedures of Au CRL, we also tried to fabricate Au-free ICLs with a structure of $C_{60}/YbO_x/MoO_x$. The low FF might be attributed to the increased sheet resistance of ICLs without Au CRL. It was found that the ICL is highly transparent over the near-infrared region, guaranteeing adequate photons reaching the NBG organic back cells (Figure 2d). Further comparison of the transmittance spectra for $C_{60}/YbO_x/Au/MoO_x$, $C_{60}/SnO_x/Au/MoO_x$, and $C_{60}/BCP/Au/MoO_x$ (Figure S7a) reveals that $C_{60}/YbO_x/Au/MoO_x$ exhibits the highest transmittance across the visible-to-near-infrared range, particularly in the NIR, thereby markedly enhancing photon harvesting in the NBG subcell. Electrically, ITO/ICL/Ag diodes display ohmic behaviour for all stacks, with $C_{60}/YbO_x/Au/MoO_x$ showing lower series resistance than its SnO_x-based counterparts (Figure S7b). Although BCP-containing ICLs exhibit slightly lower resistance, their limited thermal stability and high cost make YbO_x the optimal choice for balanced optoelectronic performance. Thereafter, the structure of ICL was selected as $C_{60}/YbO_x/Au/MoO_x$ (Figure 2e). To understand the band alignment and charge transportation mechanism in ICL, we subsequently deposited the C_{60}, YbO_x, Au, MoO_x, and PM6:Y6 blends and tested ultraviolet photoelectron spectroscopy (UPS) spectra at each layer. The characterization results are shown in Figure 2f. The gap states around the Fermi edge are detected in both YbO_x and MoO_x. These gap states would function as Anderson-Mott localized states. Different from the band transport theory, these Anderson-Mott localized states provide an effective conduction path through the

hopping mode.[43] Regarding how MoO_x thickness variations affect charge transport, we deposited MoO_x with different thicknesses and measured its UPS spectra. For ultrathin MoO_x (1–3 nm), gap states near the Fermi level enable hole transport via localized state hopping. This aligns with the Anderson-Mott model, where charge carriers bypass band transport limitations by hopping between defect states. Thicker MoO_x (5–10 nm) exhibits reduced gap state density, which can increase series resistance. However, the 1-nm Au layer in the ICL mitigates this effect by providing an alternative conductive path, ensuring balanced charge extraction. The 10-nm MoO_x thickness (used in the champion device) strikes a balance between defect-mediated transport and optical transparency, minimizing parasitic absorption while maintaining low interfacial resistance. According to Figure 2f, we depicted the energy level alignment in ICL (Figure 2g). Furthermore, a possible charge transportation and recombination mechanism is depicted.

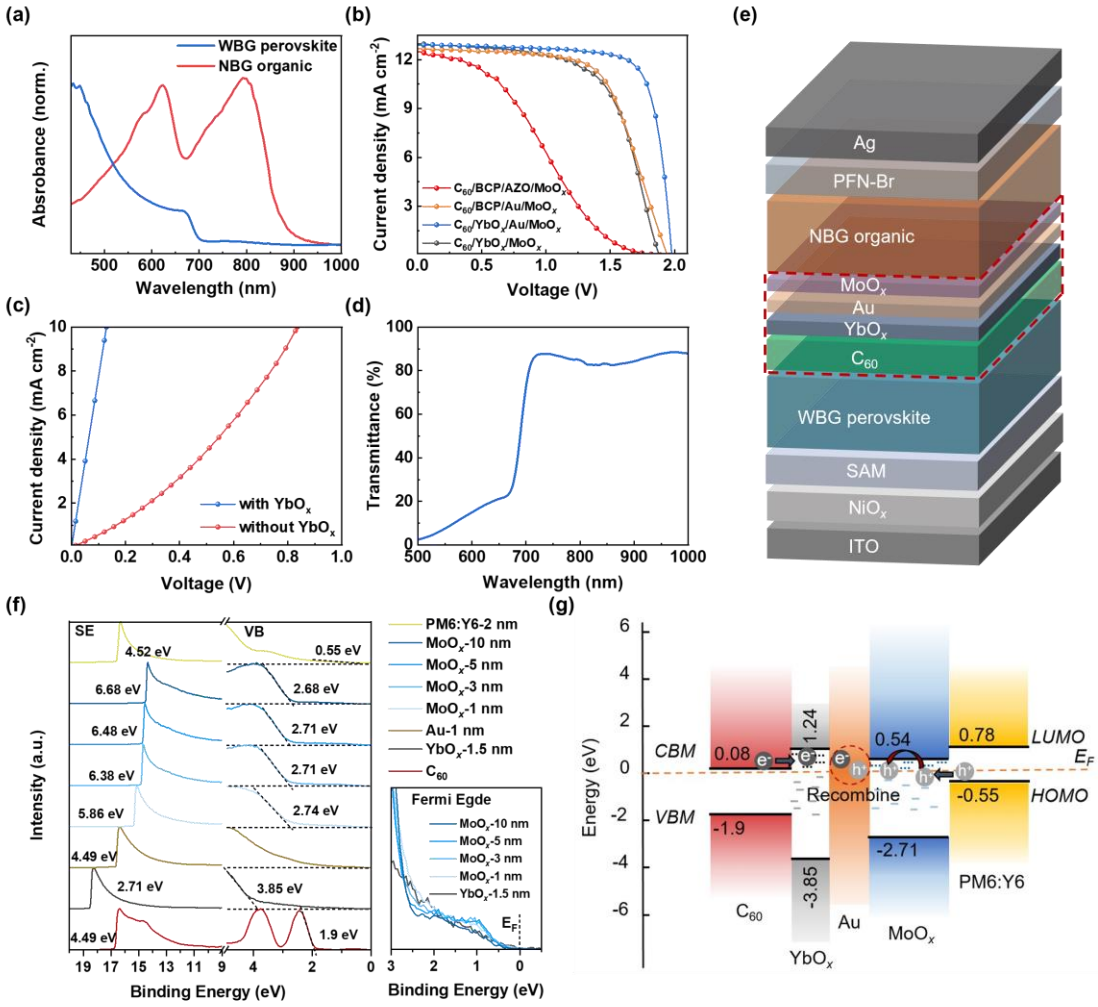

Figure 2. Design of ICL. (a) Absorption spectra of perovskite and organic absorber films. (b) *J*–*V* curves of POTSCs with different ICLs. (c) *J*–*V* characteristics of the diode devices with the structure of ITO/C_{60}/YbO_x/Au/MoO_x/Ag. (d) Transmittance spectra of a half tandem stack: ITO/NiO_x/SAM/perovskite/C_{60}/YbO_x/Au/MoO_x. (e) The device structure of a POTSC. The dashed red frame highlights the ICL (Structure: C_{60}/YbO_x/Au/MoO_x). (f) Evolution of the ultraviolet photoemission spectroscopy (UPS) spectra of the sample with subsequent deposition of C_{60}, YbO_x, Au, MoO_x, and PM6:Y6 blends. The right panel denotes the defect state of Au (1.5 nm) and MoO_x (1, 3, 5, 10 nm) based on the valence band edge. (g) The schematic illustration of charge transportation and recombination mechanism in the ICL. Note that the short gray and blue lines below the Fermi level denote the occupied gap states, while the short-dashed gray and blue lines above the Fermi level refer to the unoccupied gap states.

With the YbO_x-based ICL, the device configuration is confirmed as follows: ITO/NiO_x/SAM/ perovskite/C_{60}/YbO_x/Au/MoO_x/organic/PFN-Br/Ag. To maximize the overall performance of POTSC, it is necessary to consider the well-balanced light absorption in both WBG and NBG subcells. Here, we used the transfer matrix method (TMM) modeling to simulate the photon distribution and absorption within the device and thereby provide information guiding the device fabrication.[44-45] The key information used in the simulation is summarized in Figure S8 and Table S2. As the two subcells are connected in series, in which the J_{SC} of POTSC depends on the current-limiting subcell, it is thereby necessary to balance the photocurrent on both sides. Figure 3a presents the relation between two absorber thicknesses and J_{SC} of POTSC. It is found that the optimal thickness for perovskite and organic absorbers is 150–250 nm and 150–180 nm, when the maximized J_{SC} is ~ 14 mA cm^{-2}. Figure 3b shows the photon absorption distribution within the device based on a 260 nm perovskite and 180 nm organic absorber. We noticed that most visible photons are absorbed by the WBG perovskite, while NIR photons are absorbed by the NBG organic layer. There is a small fraction of visible photons at 550-700 nm overlapped in both the perovskite and organic absorption range, which would induce J_{SC} loss. Guided by the optical simulation results, we fabricated the POTSC with optimized absorber thicknesses, as shown in Figure 3c. Moreover, the C_{60} layer thickness is fixed at 40 nm, a value determined through a joint theoretical–experimental optimization that balances optical losses, charge-transport resistance, interfacial coverage, and overall device efficiency (Figures S9-S14). Optical modelling and experimental results confirm that the residual absorption (only about a 1% increase versus 20 nm thickness) and series resistance are acceptably small and do not compromise the high performance of the POTSCs (See detailed discussion in Supplementary Note 1).

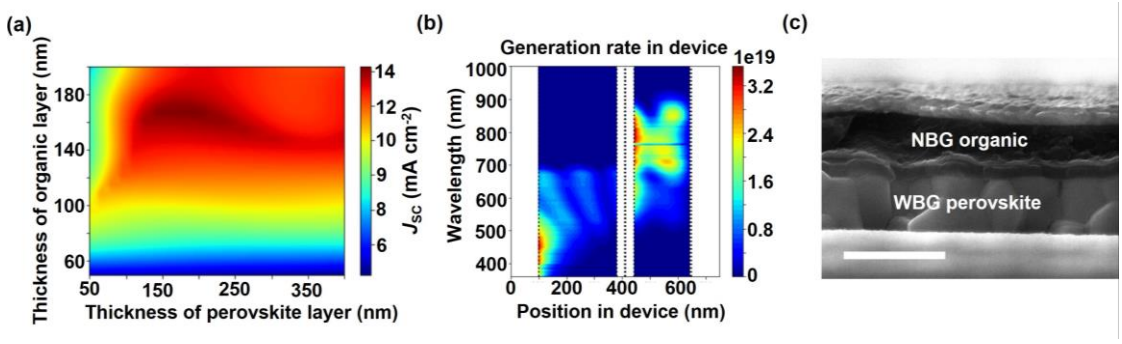

Figure 3. Optical simulation for device optimization. (a) Simulated J_{SC} as a function of the variable thicknesses of perovskite and organic absorbers under 100% internal quantum efficiency (IQE) assumption. (b) Photon absorption rate distribution within a POTSC. (c) Cross-sectional SEM image for a POTSC, scale bar, 500 nm.

The device performance of the champion POTSC is demonstrated in Figure 4a and Table 2. The champion POTSC obtains an optimal PCE of 23.2%. Notably, the POTSCs exhibit a V_{OC} of approximately 2.11 V, which is roughly equivalent to the combined individual V_{OC} values of the NBG and WBG subcells (Table 2). The voltage loss suppression stems from synergistic function of the new ICL: UPS spectra (Figure 2f) reveal gap states near the Fermi level in YbO_x and MoO_x, facilitating defect-assisted charge transport. Crucially, YbO_x insertion between C_{60} and Au reduces the electron injection barrier, establishing an ohmic contact at the ETL/CRL interface that minimizes carrier accumulation.[46] Simultaneously, MoO_x defect states enable hole transport via phonon-assisted hopping. Critically, the 1-nm Au interlayer acts as a recombination center that equilibrates electron and hole quasi-Fermi levels, suppressing interfacial potential buildup. This synergistic design yields a small voltage loss. Figure 4b provides statistics of V_{OC} for POTSC, showing decent reproducibility. The distribution of all photovoltaic parameters is shown in Figure S15. Furthermore, we have compared the performance differences between SnO_x-and YbO_x-based POTSCs (Figure S16). The results show that YbO_x-based POTSCs exhibit a higher average PCE mainly due to the enhancement of J_{SC} and FF. According to the EQE spectra (Figure 4c), the integrated J_{SC} of the front WBG perovskite subcell is 13.60 mA cm^{-2}, and the back NBG organic subcell shows an integrated J_{SC} of 13.49 mA cm^{-2}, which indicates

a small discrepancy compared to the *J*–*V* characterization results. Moreover, we tracked the PCE at the maximum power point (MPP) at a fixed voltage of 1.76 V and obtained a steady-state power output (Figure 4d). We also performed long-term MPP tracking (MPPT) measurements (Figure 4e). An encapsulated POTSC remained 82.5% of its initial PCE after 100 hours. In addition, the thermal stability of POTSCs is shown in Figure 4f. After a slight increase in PCEs at the initial stage, the tested devices underwent a drop in PCE during the following period, possibly due to the unpleasant thermal stability of WBG perovskite and NBG organic light absorbers.[7] In the end, the POTSCs retained 78% of its initial PCE after heating at 85°C for 264 h in nitrogen atmosphere. Moreover, from Figure S17, the POTSC retained 95.5% of its initial PCE after 217 days in nitrogen atmosphere without encapsulation, showcasing good storage stability.

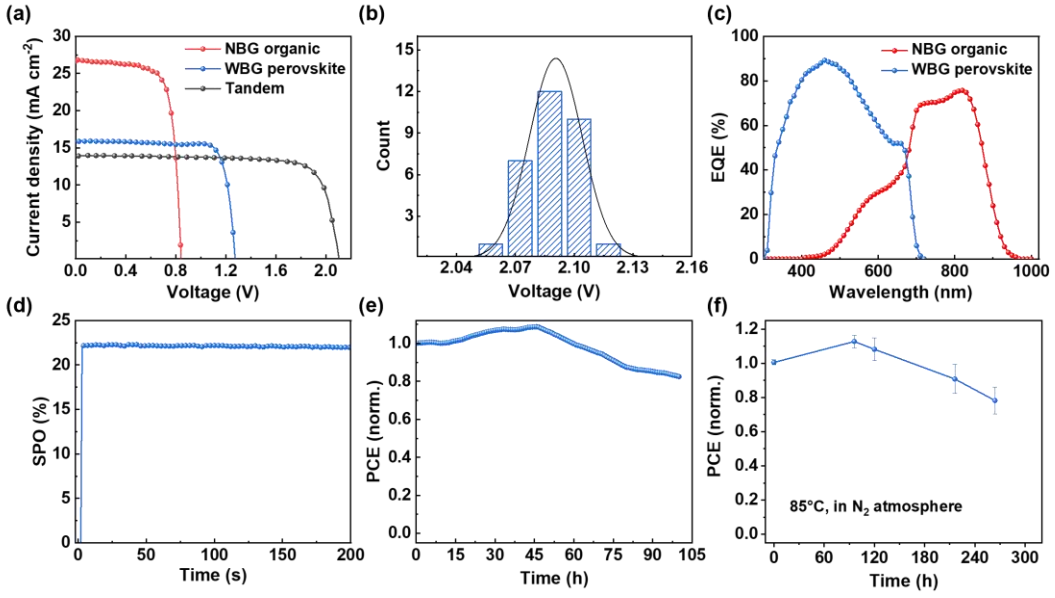

Figure 4. Device performance of POTSCs. (a) *J*–*V* curves of perovskite, organic subcells, and tandem cells. (b) V_{OC} distribution of POTSC over different batches. (c) EQE spectra of perovskite and organic subcells. (d) The steady-state power output of the champion POTSC at the maximum power point. (e) The maximum power point tracking (MPPT) curve of an encapsulated POTSC under continuous illumination by using a white LED array with an intensity of 100 mW cm^{-2} in ambient air (The surface

temperature of the tested device is about 40°C). (f) Thermal stability of non-encapsulated POTSCs in a nitrogen-filled glovebox at 85°C. The average PCEs and standard errors are obtained from five devices.

Table 2. Device performance of subcells and the champion POTSC. [a]The average values and standard deviations of the device parameters are based on 30 devices.

	V_{OC} (V)	J_{SC} (mA cm^{-2})	FF	PCE (%)
WBG perovskite	1.28	16.0	0.83	17.0
NBG organic	0.85	26.8	0.71	16.2
POTSC	2.11	13.9	0.79	23.2
	2.09 ± 0.01[a]	23.8 ± 0.2[a]	0.77 ± 0.01[a]	22.4 ± 0.31[a]

In summary, we demonstrated the effectiveness of surface treatment over WBG perovskite films in interfacial passivation and achieved a PCE of 20.1% with a V_{OC} of 1.3 V. Then, we developed an ICL design based on thermally deposited YbO_x. The insertion of YbO_x modifies the overall work function of CRL and forms the ohmic contact, facilitating charge extraction and recombination, as evidenced by the high V_{OC} and FF. The YbO_x-based ICL also exhibits high transmittance and uniform film morphology, which is beneficial for the light absorption and fabrication of the NBG organic subcell. Optical simulation analysis is carried out to balance the light absorption in both subcells. The POTSC with optimized absorber thicknesses is fabricated and achieves a PCE of 23.2% and a notable V_{OC} of 2.11 V, which is ≈99% of the summed V_{OC}s of subcells and is attributed to the effectiveness of YbO_x-based ICL. Also, the ICL can be fully thermally evaporated in a row, which is manufacturing-friendly and provides strong competitiveness in scalable production.

ASSOCIATED CONTENT

Supporting Information

The Supporting Information is available free of charge at XXXX.

Description of materials, device fabrication and characterization methods, supplementary note, SEM images, AFM images, absorption spectra, EQE_{EL} spectra, photovoltaic performance distribution, EQE spectra, transmittance spectra, I-V curves, optical constant, optical simulation, device stability, and TRPL data.

AUTHOR INFORMATION

Corresponding Authors

Peng Chen − *State Key Laboratory for Artificial Microstructure and Mesoscopic Physics, School of Physics, Frontiers Science Center for Nano-optoelectronics & Collaborative Innovation Center of Quantum Matter, Peking University, Beijing 100871, China;* Email: iamchenpeng@pku.edu.cn

Rui Zhu − *State Key Laboratory for Artificial Microstructure and Mesoscopic Physics, School of Physics, Frontiers Science Center for Nano-optoelectronics & Collaborative Innovation Center of Quantum Matter, Peking University, Beijing 100871, China; Key Laboratory for Advanced Optoelectronic Integrated Chips of Jiangsu Province, Peking University Yangtze Delta Institute of Optoelectronics, Nantong, Jiangsu 226010, China; Collaborative Innovation Center of Extreme Optics, Shanxi University, Taiyuan, Shanxi 030006, China*; orcid.org/0000-0001-7631-3589; Email: iamzhurui@pku.edu.cn

Henry J. Snaith − *Clarendon Laboratory, Department of Physics, University of Oxford, Oxford OX1 3PU, United Kingdom;* orcid.org/0000-0001-8511-790X; Email: henry.snaith@physics.ox.ac.uk

Authors

Yun Xiao − *Clarendon Laboratory, Department of Physics, University of Oxford, Oxford OX1 3PU, United Kingdom.*

Tianyu Huang − *State Key Laboratory for Artificial Microstructure and Mesoscopic Physics, School of Physics, Frontiers Science Center for Nano-optoelectronics & Collaborative Innovation Center of Quantum Matter, Peking University, Beijing 100871, China.*

Nan Chen − *School of Microelectronics, Southern University of Science and*

Technology, Shenzhen 518055, China.

Deying Luo − *International Institute for Interdisciplinary and Frontiers, Beihang University, Beijing 100191, China.*

Xin Jiang − *Beijing National Laboratory for Molecular Sciences, CAS Key Laboratory of Organic Solids, Institute of Chemistry, Chinese Academy of Sciences, Beijing 100190, China.*

Xiaohan Jia − *Cavendish Laboratory, Department of Physics, University of Cambridge, Cambridge, CB3 0HE, United Kingdom.*

Juntao Hu − *Department of Physics, Mathematics and Computer Science, Faculty of Basic Medical Science, Kunming Medical University, Kunming 650500, China.*

Dengke Wang − *Department of Physics, Center for Optoelectronics Engineering Research, Yunnan University, Kunming 650091, China.*

Pascal Kaienburg − *Clarendon Laboratory, Department of Physics, University of Oxford, Oxford OX1 3PU, United Kingdom.*

Suhas Mahesh − *Clarendon Laboratory, Department of Physics, University of Oxford, Oxford OX1 3PU; Department of Materials Science and Engineering, University of Toronto, Toronto M5S 3E4, Canada.*

Anna Jungbluth − *Clarendon Laboratory, Department of Physics, University of Oxford, Oxford OX1 3PU, United Kingdom.*

Rui Su − *Department of Materials Science and Engineering, North Carolina State University, Raleigh NC 27695, USA.*

Congmeng Li − *Institute of Electrical Engineering, Chinese Academy of Sciences, Beijing 100190, China.*

Qiang Lou − S*chool of Electronic and Computer Engineering, Peking University Shenzhen Graduate School, Shenzhen 518055, China.*

Chen Yang − *State Key Laboratory for Artificial Microstructure and Mesoscopic Physics, School of Physics, Frontiers Science Center for Nano-optoelectronics & Collaborative Innovation Center of Quantum Matter, Peking University, Beijing*

100871, China.

Bingjun Wang − *Clarendon Laboratory, Department of Physics, University of Oxford, Oxford OX1 3PU, United Kingdom.*

Irfan Habib − *Clarendon Laboratory, Department of Physics, University of Oxford, Oxford OX1 3PU, United Kingdom.*

Hao Ye − *Clarendon Laboratory, Department of Physics, University of Oxford, Oxford OX1 3PU, United Kingdom.*

Hang Zhou − *School of Electronic and Computer Engineering, Peking University Shenzhen Graduate School, Shenzhen 518055, China.*

Hui Li − *Institute of Electrical Engineering, Chinese Academy of Sciences, Beijing, 100190 China; Beijing National Laboratory for Condensed Matter Physics, Institute of Physics, Chinese Academy of Sciences, Beijing 100190, China.*

Lei Meng − *Beijing National Laboratory for Molecular Sciences, CAS Key Laboratory of Organic Solids, Institute of Chemistry, Chinese Academy of Sciences, Beijing 100190, China.*

Xiaojun Li − *Beijing National Laboratory for Molecular Sciences, CAS Key Laboratory of Organic Solids, Institute of Chemistry, Chinese Academy of Sciences, Beijing 100190, China.*

Hongyu Yu − *School of Integrated Circuits, Shenzhen Polytechnic University, Shenzhen 518055, China.*

Moritz Riede − *Clarendon Laboratory, Department of Physics, University of Oxford, Oxford OX1 3PU, United Kingdom.*

Zheng-Hong Lu − *Department of Materials Science and Engineering, University of Toronto, Toronto M5G 3E4, Canada; Department of Physics, Center for Optoelectronics Engineering Research, Yunnan University, Kunming 650091, China.*

Author Contributions

Y.X., T.H., and N.C. contributed equally to this work. All authors analyzed the data and reviewed and commented on the paper. The manuscript was written through

contributions of all authors. All authors have given approval to the final version of the manuscript.

Notes

Henry J. Snaith is the founder and Chief Scientific Officer of Oxford Photovoltaics, a company commercializing perovskite photovoltaics.

ACKNOWLEDGEMENTS

This work was financially supported by National Natural Science Foundation of China (52403369, 52325310), the National Key R&D Program of China (2021YFB3800100, 2021YFB3800101), the Yunnan Provincial Science and Technology Project at Southwest United Graduate School (202302AO370013), the China Postdoctoral Science Foundation (2020M670036, 2023TQ0009, GZB20230030), and the R&D Fruit Fund (20210001). H.J.S. and Y.X. acknowledge funding from the Engineering and Physical Science Council (EPSRC) EP/V027131/1 and GCRF grant by Research England. Y.X. acknowledges China Oxford Scholarship Fund. Y.X. acknowledges Sameer Kesava, Spencer Case, and Hanyang Ye from Oxford for their general support.

REFERENCES

1. NREL PV Research Cell Record Efficiency Chart; 2025. https://www.nrel.gov/pv/cell-efficiency (accessed 04-15-2025).

2. Chen, P.; Xiao, Y.; Li, S. D.; Jia, X. H.; Luo, D. Y.; Zhang, W.; Snaith, H. J.; Gong, Q. H.; Zhu, R., The Promise and Challenges of Inverted Perovskite Solar Cells. *Chem. Rev.* **2024,** *124*(19), 10623−10700.

3. Li, H.; Zhang, W., Perovskite Tandem Solar Cells: From Fundamentals to Commercial Deployment. *Chem. Rev.* **2020,** *120*(18), 9835−9950.

4. Jiang, X.; Qin, S.; Meng, L.; He, G.; Zhang, J.; Wang, Y.; Zhu, Y.; Zou, T.; Gong, Y.; Chen, Z., et al., Isomeric Diammonium Passivation for Perovskite-Organic Tandem Solar Cells. *Nature* **2024,** *635*(8040), 860−866.

5. Mariotti, S.; Köhnen, E.; Scheler, F.; Sveinbjörnsson, K.; Zimmermann, L.; Piot, M.; Yang, F.; Li, B.; Warby, J.; Musiienko, A., et al., Interface Engineering for High-Performance, Triple-Halide Perovskite-Silicon Tandem Solar Cells. *Science* **2023,** *381*(6653), 63−69.

6. Lin, R.; Wang, Y.; Lu, Q.; Tang, B.; Li, J.; Gao, H.; Gao, Y.; Li, H.; Ding, C.; Wen, J., et al., All-Perovskite Tandem Solar Cells with 3D/3D Bilayer Perovskite Heterojunction. *Nature* **2023,** *620*(7976), 994−1000.
7. Brinkmann, K. O.; Wang, P.; Lang, F.; Li, W.; Guo, X.; Zimmermann, F.; Olthof, S.; Neher, D.; Hou, Y.; Stolterfoht, M., et al., Perovskite-Organic Tandem Solar Cells. *Nat. Rev. Mater.* **2024,** *9*(3), 202−217.
8. Seo, S.; Park, J.-Y.; Park, J. S.; Lee, S.; Choi, D.-Y.; Kim, Y.-H.; Kim, B. J., Polymer Donors with Hydrophilic Side-Chains Enabling Efficient and Thermally-Stable Polymer Solar Cells by Non-Halogenated Solvent Processing. *Nano Res. Energy* **2024,** *3*(1), e9120088.
9. Chen, C.-C.; Bae, S.-H.; Chang, W.-H.; Hong, Z.; Li, G.; Chen, Q.; Zhou, H.; Yang, Y., Perovskite/Polymer Monolithic Hybrid Tandem Solar Cells Utilizing a Low-Temperature, Full Solution Process. *Mater. Horiz.* **2015,** *2*(2), 203−211.
10. Zhang, G.; Zhao, J.; Chow, P. C. Y.; Jiang, K.; Zhang, J.; Zhu, Z.; Zhang, J.; Huang, F.; Yan, H., Nonfullerene Acceptor Molecules for Bulk Heterojunction Organic Solar Cells. *Chem. Rev.* **2018,** *118*(7), 3447−3507.
11. Yan, C.; Barlow, S.; Wang, Z.; Yan, H.; Jen, A. K. Y.; Marder, S. R.; Zhan, X., Non-Fullerene Acceptors for Organic Solar Cells. *Nat. Rev. Mater.* **2018,** *3*(3), 18003.
12. Zhang, G.; Lin, F. R.; Qi, F.; Heumüller, T.; Distler, A.; Egelhaaf, H.-J.; Li, N.; Chow, P. C. Y.; Brabec, C. J.; Jen, A. K. Y., et al., Renewed Prospects for Organic Photovoltaics. *Chem. Rev.* **2022,** *122*(18), 14180−14274.
13. Jiang, Y.; Liu, K.; Liu, F.; Ran, G.; Wang, M.; Zhang, T.; Xu, R.; Liu, H.; Zhang, W.; Wei, Z., et al., 20.6% Efficiency Organic Solar Cells Enabled by Incorporating a Lower Bandgap Guest Nonfullerene Acceptor without Open-Circuit Voltage Loss. *Adv. Mater.* **2025,** *37*(17), 2500282.
14. Li, C.; Song, J.; Lai, H.; Zhang, H.; Zhou, R.; Xu, J.; Huang, H.; Liu, L.; Gao, J.; Li, Y., et al., Non-Fullerene Acceptors with High Crystallinity and Photoluminescence Quantum Yield Enable >20% Efficiency Organic Solar Cells. *Nat. Mater.* **2025,** *24*(3), 433−443.
15. Ma, R.; Luo, Z.; Zhang, Y.; Zhan, L.; Jia, T.; Cheng, P.; Yan, C.; Fan, Q.; Liu, S.; Ye, L., et al., Organic Solar Cells: Beyond 20%. *Sci. China Mater.* **2025,** *68*(1), 1689−1701.
16. Shang, Y.; Wang, P.; Jia, L.; Li, X.; Lian, W.; Qian, P.; Chen, M.; Chen, T.; Lu, Y.; Yang, S., Synchronous Defect Passivation of All-Inorganic Perovskite Solar Cells

Enabled by Fullerene Interlayer. *Nano Res. Energy* **2023,** *2*(3), e9120073−e9120073.
17. Yang, X.; Tu, Y.; Ye, F.; Bao, Z., Back-Contact Configuration Energizes Perovskite Photovoltaic Modules. *Nano Res. Energy* **2024,** *3*(2), e9120111.
18. Mahesh, S.; Ball, J. M.; Oliver, R. D. J.; Mcmeekin, D. P.; Nayak, P. K.; Johnston, M. B.; Snaith, H. J., Revealing the Origin of Voltage Loss in Mixed-Halide Perovskite Solar Cells. *Energy Environ. Sci.* **2020,** *13*(1), 258−267.
19. Zhang, Z.; Chen, W.; Jiang, X.; Cao, J.; Yang, H.; Chen, H.; Yang, F.; Shen, Y.; Yang, H.; Cheng, Q., et al., Suppression of Phase Segregation in Wide-Bandgap Perovskites with Thiocyanate Ions for Perovskite/Organic Tandems with 25.06% Efficiency. *Nat. Energy* **2024,** *9*(5), 592−601.
20. Wu, S.; Yan, Y.; Yin, J.; Jiang, K.; Li, F.; Zeng, Z.; Tsang, S.-W.; Jen, A. K. Y., Redox Mediator-Stabilized Wide-Bandgap Perovskites for Monolithic Perovskite-Organic Tandem Solar Cells. *Nat. Energy* **2024,** *9*(4), 411−421.
21. Chen, W.; Zhu, Y.; Xiu, J.; Chen, G.; Liang, H.; Liu, S.; Xue, H.; Birgersson, E.; Ho, J. W.; Qin, X., et al., Monolithic Perovskite/Organic Tandem Solar Cells with 23.6% Efficiency Enabled by Reduced Voltage Losses and Optimized Interconnecting Layer. *Nat. Energy* **2022,** *7*(3), 229−237.
22. Zheng, S.; Mei, X.; Chen, J.; Johansson, E. M.; Zhang, X., Colloidal Quantum Dot for Infrared-Absorbing Solar Cells: State-of-the-Art and Prospects. *Nano Res. Energy* **2024,** *3*(1), e9120095.
23. Peng, W.; Mao, K.; Cai, F.; Meng, H.; Zhu, Z.; Li, T.; Yuan, S.; Xu, Z.; Feng, X.; Xu, J., et al., Reducing Nonradiative Recombination in Perovskite Solar Cells with a Porous Insulator Contact. *Science* **2023,** *379*(6633), 683−690.
24. Li, Z.; Li, B.; Wu, X.; Sheppard, S. A.; Zhang, S.; Gao, D.; Long, N. J.; Zhu, Z., Organometallic-Functionalized Interfaces for Highly Efficient Inverted Perovskite Solar Cells. *Science* **2022,** *376*(6591), 416−420.
25. Zhang, S.; Ye, F.; Wang, X.; Chen, R.; Zhang, H.; Zhan, L.; Jiang, X.; Li, Y.; Ji, X.; Liu, S., et al., Minimizing Buried Interfacial Defects for Efficient Inverted Perovskite Solar Cells. *Science* **2023,** *380*(6643), 404−409.
26. Brinkmann, K. O.; Becker, T.; Zimmermann, F.; Kreusel, C.; Gahlmann, T.; Theisen, M.; Haeger, T.; Olthof, S.; Tückmantel, C.; Günster, M., et al., Perovskite-Organic Tandem Solar Cells with Indium Oxide Interconnect. *Nature* **2022,** *604*(7905), 280−286.
27. Yu, Z.; Yang, Z.; Ni, Z.; Shao, Y.; Chen, B.; Lin, Y.; Wei, H.; Yu, Z. J.; Holman, Z.;

Huang, J., Simplified Interconnection Structure Based on C_{60}/SnO_{2-X} for All-Perovskite Tandem Solar Cells. *Nat. Energy* **2020,** *5*(9), 657−665.
28. Chen, P.; Xiao, Y.; Hu, J.; Li, S.; Luo, D.; Su, R.; Caprioglio, P.; Kaienburg, P.; Jia, X.; Chen, N., et al., Multifunctional Ytterbium Oxide Buffer for Perovskite Solar Cells. *Nature* **2024,** *625*(7995), 516−522.
29. Man, J.-X.; Hu, J.-T.; Wang, D.-K.; He, S.-J.; Lu, Z.-H., Ytterbium Oxide Electron Injection Interface in Organic Light-Emitting Diode. *Appl. Phys. Lett.* **2022,** *120*(12), 121101.
30. McMeekin, D. P.; Sadoughi, G.; Rehman, W.; Eperon, G. E.; Saliba, M.; Hörantner, M. T.; Haghighirad, A.; Sakai, N.; Korte, L.; Rech, B., A Mixed-Cation Lead Mixed-Halide Perovskite Absorber for Tandem Solar Cells. *Science* **2016,** *351*(6269), 151−155.
31. Bai, S.; Da, P.; Li, C.; Wang, Z.; Yuan, Z.; Fu, F.; Kawecki, M.; Liu, X.; Sakai, N.; Wang, J. T., et al., Planar Perovskite Solar Cells with Long-Term Stability Using Ionic Liquid Additives. *Nature* **2019,** *571*(7764), 245−250.
32. Wang, F.; Duan, D.; Singh, M.; Sutter‐Fella, C. M.; Lin, H.; Li, L.; Naumov, P.; Hu, H., Ionic Liquid Engineering in Perovskite Photovoltaics. *Energy Environ. Mater.* **2022,** *6*(5), e12435.
33. Chen, H.; Teale, S.; Chen, B.; Hou, Y.; Grater, L.; Zhu, T.; Bertens, K.; Park, S. M.; Atapattu, H. R.; Gao, Y. J., et al., Quantum-Size-Tuned Heterostructures Enable Efficient and Stable Inverted Perovskite Solar Cells. *Nat. Photonics* **2022,** *16*(5), 352−358.
34. Zhou, L.; Lin, Z.; Ning, Z.; Li, T.; Guo, X.; Ma, J.; Su, J.; Zhang, C.; Zhang, J.; Liu, S., et al., Highly Efficient and Stable Planar Perovskite Solar Cells with Modulated Diffusion Passivation Towards High Pce and Ultra‐High Fill Ffactor. *Solar RRL* **2019,** *3*(1), 1900293.
35. Zhao, L.; Li, Q.; Hou, C.-H.; Li, S.; Yang, X.; Wu, J.; Zhang, S.; Hu, Q.; Wang, Y.; Zhang, Y., et al., Chemical Polishing of Perovskite Surface Enhances Photovoltaic Performances. *J. Am. Chem. Soc.* **2022,** *144*(4), 1700−1708.
36. Chen, P.; Hu, J.; Yu, M.; Li, P.; Su, R.; Wang, Z.; Zhao, L.; Li, S.; Yang, Y.; Zhang, Y., et al., Refining Perovskite Heterojunctions for Effective Light-Emitting Solar Cells. *Adv. Mater.* **2023,** *35*(3), 2208178.
37. Luo, D. Y.; Su, R.; Zhang, W.; Gong, Q. H.; Zhu, R., Minimizing Non-Radiative Recombination Losses in Perovskite Solar Cells. *Nat. Rev. Mater.* **2020,** *5*(1), 44−60.
38. Green, Martin A.; Dunlop, Ewan D.; Yoshita, M.; Kopidakis, N.; Bothe, K.; Siefer,

G.; Hao, X.; Jiang, Jessica Y., Solar Cell Efficiency Tables (Version 65). *Prog. Photovolt.: Res. Appl.* **2024,** *33*(1), 3−15.

39. An, Y.; Zhang, N.; Zeng, Z.; Cai, Y.; Jiang, W.; Qi, F.; Ke, L.; Lin, F. R.; Tsang, S. W.; Shi, T., et al., Optimizing Crystallization in Wide-Bandgap Mixed Halide Perovskites for High-Efficiency Solar Cells. *Adv. Mater.* **2023,** *36*(17), 2306568.

40. Cheng, M.; Duan, Y.; Zhang, D.; Xie, Z.; Li, H.; Cao, Q.; Qiu, Z.; Chen, Y.; Peng, Q., Tailoring Buried Interface and Minimizing Energy Loss Enable Efficient Narrow and Wide Bandgap Inverted Perovskite Solar Cells by Aluminum Glycinate Based Organometallic Molecule. *Adv. Mater.* **2025,** *37*(10), 2419413.

41. Yuan, J.; Zhang, Y. Q.; Zhou, L. Y.; Zhang, G. C.; Yip, H. L.; Lau, T. K.; Lu, X. H.; Zhu, C.; Peng, H. J.; Johnson, P. A., et al., Single-Junction Organic Solar Cell with over 15% Efficiency Using Fused-Ring Acceptor with Electron-Deficient Core. *Joule* **2019,** *3*(4), 1140−1151.

42. Chen, X.; Jia, Z.; Chen, Z.; Jiang, T.; Bai, L.; Tao, F.; Chen, J.; Chen, X.; Liu, T.; Xu, X., et al., Efficient and Reproducible Monolithic Perovskite/Organic Tandem Solar Cells with Low-Loss Interconnecting Layers. *Joule* **2020,** *4*(7), 1594−1606.

43. Chen, N.; Man, J.; Zhang, D.; Wang, D.; Hu, J.; Shi, C.; Lu, Z.-H., Yb_2O_3/MoO_3 Connecting Electrodes for Tandem Organic Semiconductor Devices. *Phy. Rev. Applied* **2024,** *22*(5), 054015.

44. Burkhard, G. F.; Hoke, E. T.; McGehee, M. D., Accounting for Interference, Scattering, and Electrode Absorption to Make Accurate Internal Quantum Efficiency Measurements in Organic and Other Thin Solar Cells. *Adv. Mater.* **2010,** *22*(30), 3293−3297.

45. Sun, S. Q.; Xu, X.; Sun, Q.; Yao, Q.; Cai, Y.; Li, X. Y.; Xu, Y. L.; He, W.; Zhu, M.; Lv, X., et al., All-Inorganic Perovskite-Based Monolithic Perovskite/Organic Tandem Solar Cells with 23.21% Efficiency by Dual-Interface Engineering. *Adv. Energy Mater.* **2023,** *13*(16), 2204347.

46. Meng, L.; Ding, L.; Zhang, Y.; Wan, X.; Li, C.; Zhang, X.; Wang, Y.; Ke, X.; Xiao, Z.; Xia, R., et al., Organic and Solution-Processed Tandem Solar Cells with 17.3% Efficiency. *Science* **2018,** *361*(6407), 1094−1098.